Chemical Engineering and Processing 77 (2014) 50–65

Contents lists available at ScienceDirect

Chemical Engineering and Processing: Process Intensification

journal homepage: www.elsevier.com/locate/cep

Heterogeneous modeling of an autothermal membrane reactor coupling dehydrogenation of ethylbenzene to styrene with hydrogenation of nitrobenzene to aniline: Fickian diffusion model

Nabeel S. Abo-Ghander[a], Filip Logist[b], John R. Grace[a,*], Jan F.M. Van Impe[b], Said S.E.H. Elnashaie[a], C. Jim Lim[a]

[a] Chemical and Biochemical Engineering Department, University of British Columbia, Vancouver, Canada V6T 1Z3
[b] BioTeC and OPTEC, Chemical Engineering Department, KU Leuven, W. de Croylaan 46, B-3001 Leuven, Belgium

ARTICLE INFO

Article history:
Received 2 August 2012
Received in revised form
17 December 2013
Accepted 30 December 2013
Available online 18 January 2014

Keywords:
Integrated catalytic membrane reactor
Dehydrogenation
Hydrogenation
Heterogeneous model
Fickian model
Effectiveness factors

ABSTRACT

Coupling of reactions in catalytic membrane reactors provides a route to process intensification. Dehydrogenation of ethylbenzene and hydrogenation of nitrobenzene form a promising pair of processes to be coupled in a membrane reactor. The heat released from the hydrogenation side is utilized to break the endothermality on the dehydrogenation side, while hydrogen produced on the dehydrogenation side permeates through the hydrogen-selective membranes, enhances the equilibrium conversion of ethylbenzene and reacts with nitrobenzene on the permeate side to produce aniline. Mathematical reactor models are excellent tools to evaluate the extent of improvement before experiments are set up. However, a careful selection of phenomena considered by the reactor model is needed in order to obtain accurate model predictions.

To investigate the effect of the intraparticle resistances on the performance of the cocurrent configuration of the coupling reactor, a heterogeneous fixed bed reactor model is developed with Fickian diffusion inside the catalyst pellets. For the condition of interest, the styrene yield is found to be 82% by the homogenous model, 73% by the heterogeneous model for isothermal pellets, and 69% by the heterogeneous model with non-isothermal pellets. Hence, the homogeneous model overestimates the yield by 5–15% of their actual values.

1. Introduction

Coupling of reactions in a single reactor can be very beneficial, offering a number of advantages such as eliminating unnecessary heat transfer units [1], reducing overall heat losses, cost savings [2] and significant gains in yield and/or conversions due to shifting the thermodynamic equilibrium conversion by continuously removing one of the reaction products and supplying heat to the endothermic reactions [3]. As a result, these reactors are excellent examples of process integration and intensification.

In the last two decades, a number of studies have appeared addressing the usefulness of reaction coupling. An interesting reaction for this purpose involves the dehydrogenation of ethylbenzene to styrene. Abdalla and Elnashaie [4] developed a rigorous model to describe the behavior of a membrane reactor in which ethylbenzene was dehydrogenated to styrene. The dusty gas model was used to describe the diffusion inside the catalyst pellets. Later, this model was used to extract intrinsic kinetics from data obtained from an industrial reactor and to investigate the potential economic advantages of a hydrogen-selective membrane. It was found that a membrane reactor could considerably improve the ethylbenzene conversion, and the yield and selectivity of styrene. Abdalla and Elnashaie [5] studied the effect of the sweep gas flow rates in a catalytic membrane reactor in which dehydrogenation of ethylbenzene to styrene took place. An appreciable enhancement in ethylbenzene conversion, styrene yield and selectivity were observed in the proposed membrane reactor. Abdalla and Elnashaie [6] proposed a fluidized bed with and without a selective membrane for dehydrogenating ethylbenzene to styrene. Different design and operating parameters, i.e. bubble diameter, steam-to-ethylbenzene ratio, feed temperature, and number of fluidized beds in series, were investigated. It was demonstrated that a careful choice of those parameters could improve the ethylbenzene conversion and styrene yield compared to industrial fixed bed reactors. Hermann et al. [7] studied dehydrogenation of ethylbenzene to styrene in a composite Pd/porous stainless steel membrane fixed bed reactor. A model was presented in which different types of diffusion were considered. After adjusting the kinetics available to

* Corresponding author. Fax: +1 604 822 6003.
E-mail address: jgrace@chbe.ubc.ca (J.R. Grace).

0255-2701/$ – see front matter © 2014 Elsevier B.V. All rights reserved.
http://dx.doi.org/10.1016/j.cep.2013.12.009

Notation

a_i	constant, 1 for hydrogen, 0 otherwise
A_{cs}, A'_{cs}	area-equivalent diameter of shell and tube side (m^2)
C_i, C'_i	concentration of i inside the catalyst pellet on shell and tube sides (mol/m^3).
C_{is}, C'_{is}	concentration of i at the surface of catalyst pellet on shell and tube sides (mol/m^3)
Cp_i, Cp'_i	heat capacity of component i on shell and tube side (J/mol/K)
D	area-equivalent diameter on shell side (m)
D_{ie}	effective diffusivity of component i (m^2/s)
D_{im}	diffusivity of component i into mixture (m^2/s)
D_{ik}	Knudsen diffusivity of component i (m^2/s)
D^e_{im}	effective diffusivity of component i into mixture (m^2/s)
D^e_{ik}	effective Knudsen diffusivity of component i (m^2/s)
D_p, D'_p	diameter of catalyst particle on shell and tube side (m)
D_t	diameter of tube (m)
E_j	activation energy of reaction j on shell side (J/mol/K)
E'	activation energy of hydrogenation reaction on tube side (J/mol/K)
G, G'	mass velocity on shell and tube side (kg/m^2)
g_c	conversion factor equal to 1.0 in metric unit
H_i, H'_i	enthalpy of component i on shell and tube side (J/mol)
h, h'	convective heat transfer coefficients of gas mixture on shell and tube side ($J/s/m^2/K$)
k, k'	thermal conductivities of catalyst particle on shell and tube side (J/s/m/K)
k_g, k'_g	thermal conductivities of gas mixture on shell and tube side (J/s/m/K)
k_{io}	reaction i pre-exponential factor ($mol/K^m/kg\,cat/s/bar^n$), (for k_1 and k_2, $m=0$, $n=1$; for k_3 and k_5, $m=0$, $n=2$; for k_4, $m=0$, $n=1.5$; for k_6, $m=3$, $n=3$)
k_i	reaction i rate constant ($mol/K^m/kg\,cat/s/bar^n$), (for k_1 and k_2, $m=0$, $n=1$; for k_3 and k_5, $m=0$, $n=2$; for k_4, $m=0$, $n=1.5$; for k_6, $m=3$, $n=3$)
L	total length of reactor (m)
N	number of tubes in hybrid reactor
n_{EBo}	feed molar flowrates of ethylbenzene on shell side (mol/s)
n_{NBo}	feed molar flowrates of nitrobenzene on tube side (mol/s)
n_i, n'_i	molar flow rate of component i on shell and tube side (mol/s)
J_i	molar flux of component i ($mol/m^2/s$)
p_i, p'_i	partial pressure of component i on shell and tube side (bar), partial pressure of component i on tube side (bar)
P, P'	total pressure on shell side and tube side of reactor (bar)
P_f, P'_f	feed pressure on shell side and tube side (bar)
Q	heat transferred from one tube side to shell side (J/m)
Q_o	pre-exponential constant of hydrogen membrane ($mol/m/s/bar^{0.5}$)
R_p	radius of the catalyst pellets on shell side (m)
r_j	rate of reaction j on shell side ($mol/kg\,cat/s$)
r'	rate of reaction on tube side ($mol/kg\,cat/s$)
r_1	inner radius of hydrogenation tube (m)
r_2	outer radius of hydrogenation tube (m)
$r_3 - r_2$	thickness of palladium membrane (m)
T, T'	temperature on shell and tube side of reactor (K)
T_s, T'_s	temperature at the surface of catalyst pellets on shell and tube side of reactor (K)
X_{NB}	conversion of nitrobenzene on tube side
y, y'	radial position inside the catalyst pellet (m)
Y_{ST}	yield of styrene
z	axial coordinate along reactor (m)
$[\Delta H(T)]_j$	heat of reaction j at temperature T on shell side (J/mol)
$[\Delta H'(T')]$	heat of reaction at temperature T' on tube side (J/mol)
μ_g, μ'_g	viscosity of gas mixture on shell and tube side (Pa.s)
ω	dimensionless radial distance inside catalyst pellets on dehydrogenation and hydrogenation sides
ε, ε'	porosity of catalyst particle on shell and tube side
τ, τ'	tortuosity of catalyst particle on shell and tube side
ρ_s, ρ'_s	catalyst solid density on shell and tube side (kg/m^3)
σ_{ij}	stoichiometric coefficient of reactant i in reaction j
δ_{H_2}	thickness of hydrogen permeation membrane (m)
η_j, η'_j	effectiveness factor for reaction j and hydrogenation reaction on shell and tube side
η^H_j	effectiveness factor for heat released or absorbed due to reaction j

match the conversion and selectivity, the model predicted more than 90% ethylbenzene conversion as the pressure increased, with no observable decrease in styrene selectivity.

Elnashaie et al. [8] mathematically coupled dehydrogenation of ethylbenzene to styrene with hydrogenation of benzene to cyclohexane in a membrane fixed bed reactor. This study replaced the sweep gas on the shell side with a second useful reaction to produce another useful product, i.e. benzene. Both cocurrent and countercurrent configurations of the membrane reactor were considered, with kinetics of four different catalysts, one being an industrial catalyst. With commercial membranes, the new configured reactor was predicted to give 79% ethylbenzene conversion, and 72% styrene yield, significantly higher than for the industrial fixed bed reactor. Mustafa and Elnashaie [9] investigated coupling dehydrogenation of ethylbenzene with the hydrogenation of benzene in a membrane reactor. A rigorous mathematical model was developed in which intraparticle diffusion on both sides was considered. In the hybrid reactor, the predicted yield of styrene was as high as 87%. Abashar [3] studied the coupling of the same two reactions, but in a fixed bed reactor. The reactor chamber contained intermingled dehydrogenation and hydrogenation catalysts. A number of the operating parameters were examined, and a substantial increase in ethylbenzene conversion was predicted in the new fixed bed reactor.

Abo-Ghander et al. [10] modeled coupling of dehydrogenation of ethylbenzene to styrene with hydrogenation of nitrobenzene to aniline in a shell-and-tube autothermal reactor. The model included for the first time heat transfer across the membrane due to hydrogen diffusion, as well as due to conduction. Both cocurrent and countercurrent configurations were examined, and substantial enhancement was predicted compared to the fixed bed reactor. For the operating conditions investigated, the conversion reached 23.4% for the uncoupled adiabatic fixed bed case, 54.6% for the cocurrent membrane reactor, and 61.7% for the membrane reactor in a countercurrent flow configuration. The styrene yield predicted for the uncoupled adiabatic fixed bed was 18.9%. For the membrane reactor, the predicted yield increased to 52.5% for the cocurrent flow configuration and 57.7% for the countercurrent case. Apart

from membrane reactors, other forms and concepts of reaction coupling, such as coupling endothermic reactions with exothermic ones for efficient utilization of energy, have also been considered [2,11–15].

These studies indicate that component effectiveness factors can play a significant role for dehydrogenation of ethylbenzene to styrene in fixed bed reactors. As a result, the homogenous model of Abo-Ghander et al. [10] should be adjusted to consider the catalyst intraparticle diffusion on both sides of the membrane reactor. To achieve this aim, a model based on Fickian diffusion is used in this paper to model diffusion inside the catalyst pellets on both sides of the membrane. This new model is then used: (*i*) to study the molar flow rates of selected key components and temperature profiles compared with those from the homogeneous model; (*ii*) to evaluate the performance of optimal reactor designs in terms of the styrene yield on the dehydrogenation side, conversion of nitrobenzene on the hydrogenation side, and temperature profiles on both sides of the reactor.

The paper is structured as follows. Section 2 introduces the reactor configuration and presents the thermodynamic and kinetic information of all relevant reactions. Section 3 elaborates on the balance equations for the gas and the catalyst phase. On both the hydrogenation and the dehydrogenation side, mass balances for the different reaction species, as well as the energy and momentum balances, are derived and suitable connection terms are added. Also details about the computational procedure are provided. Section 4 presents and discusses the simulation results.

2. Reactor configuration

The configuration of interest is portrayed in Fig. 1. In the shell compartment packed with catalyst particles, ethylbenzene (EB) is dehydrogenated to produce styrene (ST) as the main product; benzene (BZ), toluene (TO), ethylene and other light gases are side products. The chemical equations representing the reactions are (see also Eqs. (1)–(6) in [10]):

$$C_6H_5CH_2CH_3 \leftrightarrow C_6H_5CHCH_2 + H_2 \qquad \Delta H_{298} = 117.6\,\text{kJ/mol} \quad (1)$$

$$C_6H_5CH_2CH_3 \rightarrow C_6H_6 + C_2H_4 \qquad \Delta H_{298} = 105.4\,\text{kJ/mol} \quad (2)$$

$$C_6H_5CH_2CH_3 + H_2 \rightarrow C_6H_5CH_3 + CH_4 \qquad \Delta H_{298} = -54.6\,\text{kJ/mol} \quad (3)$$

$$2H_2O + C_2H_4 \rightarrow 2CO + 4H_2 \qquad \Delta H_{298} = 210.2\,\text{kJ/mol} \quad (4)$$

$$H_2O + CH_4 \rightarrow CO + 3H_2 \qquad \Delta H_{298} = 206.1\,\text{kJ/mol} \quad (5)$$

$$H_2O + CO \rightarrow CO_2 + H_2 \qquad \Delta H_{298} = -41.2\,\text{kJ/mol} \quad (6)$$

The first reaction in this network is the main reversible, endothermic one. From Le Chatelier's principle, the forward reaction, i.e. production of styrene, is favored by operating at low pressure and high temperature.

Hydrogen produced in this compartment diffuses through palladium hydrogen-selective-membrane walls to the inside of cylindrical tubes extending along the reactor. The tube walls are permeable to hydrogen, with a layer of stainless steel of a thickness of 1.2 mm coated with a palladium layer of thickness 25 μm. The Palladium supported on palladium stainless steel membrane is completely selective toward hydrogen permeation. On the tube side, the diffused hydrogen reacts with nitrobenzene (NB) to produce aniline (AN):

$$C_6H_5NO_2 + 3H_2 \rightarrow C_6H_5NH_2 + 2H_2O \qquad \Delta H_{298} = -443.0\,\text{kJ/mol} \quad (7)$$

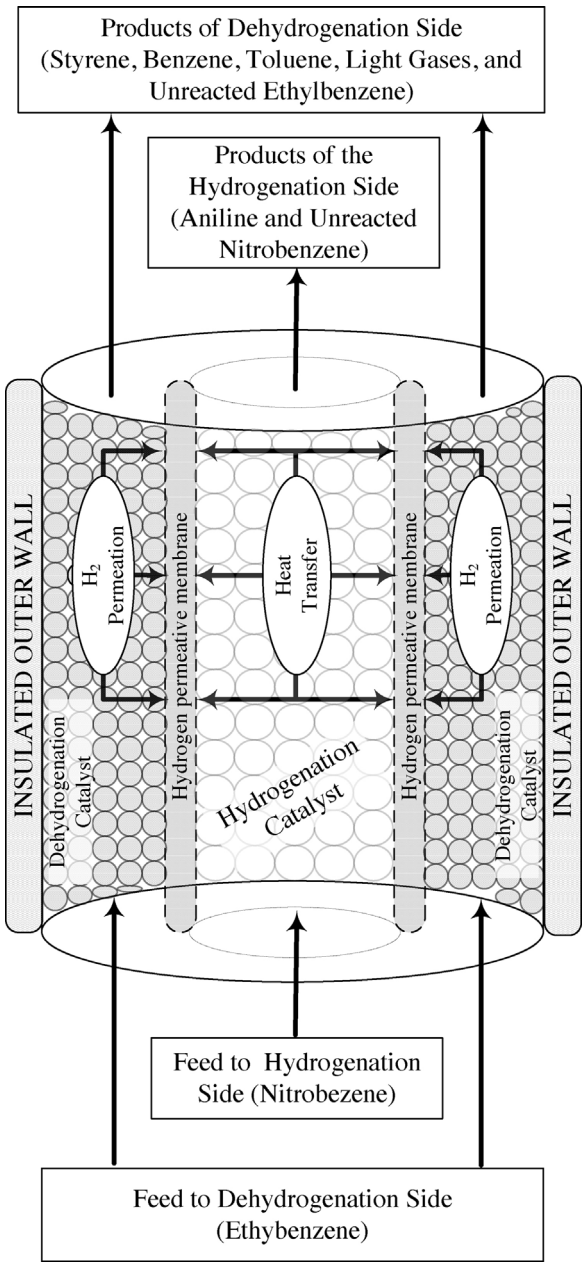

Fig. 1. Schematic of the integrated membrane fixed bed reactor.

This reaction is irreversible and highly exothermic (see also Eq. (7) in [10]). Abo-Ghander et al. [10] showed that coupling these two reactions, i.e. dehydrogenation of ethylbenzene with the hydrogenation of nitrobenzene, could be very beneficial. Removing hydrogen from the dehydrogenation side and providing heat to the same side from the hydrogenation heat of reaction were predicted to play very important roles in increasing the styrene yield. The external wall of the coupled reactor is treated as adiabatic, a reasonable assumption due to the small surface area-to-volume ratio. Expressions for the rate of reactions and numerical values for the pre-exponential constants and activation energies are listed in Tables 1 and 2. Similar values can be found in Tables 1 and 2 of [10,20]. The shell side of this reactor is assumed to be packed with an iron oxide (Fe_2O_3) catalyst promoted with potassium carbonate (K_2CO_3) and chromium oxide (Cr_2O_3) while the tube side is packed with a palladium catalyst supported on an α-alumina carrier. In

Table 1
Stoichiometric equations, heats of reactions and reaction rate expressions for reactions considered.

Chemical reaction	Heat of reaction	Kinetic equation	Reference
Dehydrogenation side[a]			
$C_6H_5CH_2CH_3 \leftrightarrow C_6H_5CHCH_2 + H_2$	$\Delta H_{298} = 117.6$ kJ/mol	$r_1 = k_1\left(p_{EB} - p_{ST}\frac{p_{H_2}}{K_A}\right)$	[16]
$C_6H_5CH_2CH_3 \rightarrow C_6H_6 + C_2H_4$	$\Delta H_{298} = 105.4$ kJ/mol	$r_2 = k_2 p_{EB}$	[16]
$C_6H_5CH_2CH_3 + H_2 \rightarrow C_6H_5CH_3 + CH_4$	$\Delta H_{298} = -54.6$ kJ/mol	$r_3 = k_3 p_{EB} p_{H_2}$	[16]
$2H_2O + C_2H_4 \rightarrow 2CO + 4H_2$	$\Delta H_{298} = 210.2$ kJ/mol	$r_4 = k_4 p_{H_2O} p_{C_2H_4}^{1/2}$	[16]
$H_2O + CH_4 \rightarrow CO + 3H_2$	$\Delta H_{298} = 206.1$ kJ/mol	$r_5 = k_5 p_{H_2O} p_{CH_4}$	[16]
$H_2O + CO \rightarrow CO_2 + H_2$	$\Delta H_{298} = -41.2$ kJ/mol	$r_6 = k_6\left(\frac{p}{T^3}\right) p_{H_2O} p_{CO}$	[16]
Hydrogenation side[b]			
$C_6H_5NO_2 + 3H_2 \rightarrow C_6H_5NH_2 + 2H_2O$	$\Delta H_{298} = -443.0$ kJ/mol	$r' = \frac{k' K_{NB} K_{H_2} p'_{NB} \sqrt{p'_{H_2}}}{\left(1 + K_{NB} p'_{NB} + K_{H_2}\sqrt{p'_{H_2}}\right)^2}$	[17]

[a] Partial pressure in bars.
[b] Partial pressure in kPa.

summary, this section has introduced all necessary thermodynamic and kinetic information.

3. Reactor model

This section introduces the balance equations for both phases and both reactor sides (i.e. shell and tube side, respectively). First the gas phase is considered and second the catalyst particles are looked at. Each time, first the underlying assumptions are clearly listed, while afterwards the mathematical equations are detailed. Suitable relations to connect the reactor compartments as well as to connect the two phases are also introduced. The overall computational procedure and the software used to perform the calculations are summarized at the end of the section.

The differential equations governing the behavior of the catalytic membrane reactor coupling dehydrogenation of ethylbenzene with hydrogenation of nitrobenzene are based the following assumptions:

1. Steady-state operation.
2. Ideal gas behavior in both the tubes and shell of the reactor.
3. Plug flow for the fixed beds on both shell and tube sides.
4. Heterogeneous model, i.e. significant gradients in concentrations/temperatures inside the catalyst pellets.
5. The flow rates on both sides are high enough to minimize the external mass and heat transfer resistances. Hence, only intraparticle diffusion needs to be considered.
6. The reactor external wall is adiabatic.
7. Catalyst deactivation is neglected.
8. Pressure gradients in both the shell and tubes are based on Ergun's equation.
9. Spherical catalyst pellets.
10. Cocurrent flow in the shell and tubes.

Table 2
Frequency factors and activation energies for reactions considered.

Reaction	k_{io} [a]	E_i (kJ/kmol)	Reference
1[b]	8.32×10^3	0.909×10^5	
2	4.23×10^9	2.080×10^5	
3	6.13×10^3	0.915×10^5	[16]
4	3.95×10^3	1.040×10^5	
5	1.42×10^2	0.657×10^5	
6	5.80×10^{12}	0.736×10^5	
7[c]	1.86×10^{-4}	10.0×10^3	[17]

[a] $k_i = (10/36)k_{io}\exp(-(E_i/RT))$, where k_{io} is the pre-exponential factor for $1 \le i \le 6$. $k_i = 10^3 k_{io}\exp(-(E_i/RT))$, for $i = 7$.
[b] The equilibrium constant is calculated by: $K_A = \exp(-\Delta F/RT)$, where: $\Delta F = a + bT + cT^2$, $a = 122725.16$, $b = -126.27/K$, $c = -2.194 \times 10^{-3}/K^2$.
[c] $K_{NB} = 1.51 \times 10^{-2}$ kPa, $K_{H_2} = 0.14$ kPa$^{-0.5}$.

The reactor model differential equations are derived by considering an infinitesimal element inside the reactor through which both moles and energy flow. Hydrogen diffuses from the dehydrogenation side to the hydrogenation side, whereas heat is transferred from the hydrogenation to the dehydrogenations side. The reactor model Eqs. (8)–(15) and rates of both hydrogen diffusion and heat transfer per unit length are given in Table 3. In this table mass balances (Eq. (8) and (11)) for the hydrogenation and dehydrogenation side have been adopted for the reacting components based on the balances in Eqs. (8) and (11) of [20] and their extensions in Eqs. (8) and (11) in [10]. Similarly the energy balances (Eqs. (9) and (12)) for both sides correspond to Eqs. (9) and (12) in [20] and their extended versions in Eqs. (9) and (12) in [20]. The Eqs. (10) and (13) describing the pressure evolution on both sides are identical to the ones (i.e. Eqs. (10) and (13)) in [10,20]. Transfer of hydrogen and heat across the membrane is described by Eqs. (14) and (15) in a similar way by Eqs. (14) and (15) in [10,20].

The model equations describing the diffusion inside the catalyst pellets are based on the following assumptions.

1. Steady-state molar and energy flow.
2. The porous structure of all catalyst pellets is homogeneous.
3. Ideal gas law.
4. The concentration and temperature profiles are symmetrical around the center of the spherical catalyst particles.
5. External mass and heat transfer resistances are negligible
6. Negligible viscous flow inside the pellets inducing isobaric diffusion.
7. Convective diffusion is neglected; only ordinary molecular and Knudsen diffusion are significant.
8. Diffusion is represented by Fick's law with the component diffusion coefficient obtained from molecular diffusion and Knudsen diffusion coefficients.
9. For mathematical simplicity, the variation of the effective component diffusivity coefficient along the radial direction is negligible.
10. Heat flux introduced by species, i.e. Dufour effect, is negligible.
11. Thermal conductivities of the catalyst pellets on both the shell and tube sides of the reactor are assumed to be constant.

Table 3
Model equations for coupled catalytic membrane reactor.

Balance equations	Mathematical expressions	
Dehydrogenation side		
Mole	$\frac{dn_i}{dz} = \sum_{j=1}^{6} \sigma_{ij} \left(3 \int_0^{1.0} r_j \omega^2 d\omega \right) (1-\varepsilon) A_{cs} \rho_s - 2\pi r_3 N a_i J_i$	(8)
Energy	$\frac{dT}{dz} = \frac{\sum_{j=1}^{6} \left(3 \int_0^{1.0} [-\Delta H(T)]_j r_j \omega^2 d\omega \right) (1-\varepsilon) A_{cs} \rho_s + NQ}{\sum_{i=1}^{10} n_i Cp_i}$	(9)
Pressure	$\frac{dP}{dz} = -\frac{G}{\rho_g g_c D_p} \left(\frac{1-\varepsilon}{\varepsilon^3} \right) \left[\frac{150(1-\varepsilon)\mu_g}{D_p} + 1.75G \right]$	(10)
Hydrogenation side		
Mole	$\frac{dn'_i}{dz} = \sigma_i \left(3 \int_0^{1.0} r' \omega'^2 d\omega' \right) (1-\varepsilon') A'_{cs} \rho'_s + 2\pi\, r_3 a_i J_i$	(11)
Energy	$\frac{dT'}{dz} = \frac{(2\pi\, r_3) \sum_{i=1}^{i} a_i J_i \int_{T'}^{T} Cp_i dT + \left(3 \int_0^{1.0} [-\Delta H'(T')]\, r' \omega'^2 d\omega' \right) (1-\varepsilon') A'_{cs} \rho'_s - Q}{\sum_{i=1}^{4} n'_i Cp'_i}$	(12)
Pressure	$\frac{dP'}{dz} = -\frac{G'}{\rho'_g g_c D'_p} \left(\frac{1-\varepsilon'}{\varepsilon'^3} \right) \left[\frac{150(1-\varepsilon')\mu'_g}{D'_p} + 1.75G' \right]$	(13)
Diffusion of hydrogen across membrane	$J_{H_2} = \frac{Q_o \exp(-E_{H_2,P}/RT)}{\delta_{H_2}} \left(\sqrt{P_{H_2}} - \sqrt{P'_{H_2}} \right)$ where: $Q_o = 7.29 \times 10^{-3}$ (mol × m)/(m² × min × atm$^{0.5}$), $\delta_{H_2} = 25 \times 10^{-6}$ m, $E_{H_2,P} = 20.5 \times 10^3$ J/mol	(14)
Heat transfer across membrane	$Q = \frac{2\pi\, r_1 (T' - T)}{[(1/h') + (r_1/k_{ss}) \ln(r_2/r_1) + (r_1/k_{Pd}) \ln(r_3/r_2) + (r_1/r_2 h)]}$ where: $k_{ss} = 22.88$ W/m × K, $k_{Pd} = 93.3$ W/m × K $\frac{hD_t}{k_g} = 0.813 \left(\frac{D_p G}{\mu_g} \right)^{0.9} \exp\left(-\frac{6D_p}{D_t} \right)$ $\frac{h' D'_t}{k'_g} = 3.50 \left(\frac{D'_p G'}{\mu'_g} \right)^{0.7} \exp\left(-\frac{4.6 D'_p}{D'_t} \right)$	(15)

To derive the catalyst model equations, a small spherical shell inside the catalyst pellets is considered across which both moles and heat flow, as shown in Fig. 2. Applying the balance equations, and expressing the molar flux using Fick's law leads to the following.

Catalyst mole balance equation on dehydrogenation side:

$$\frac{d^2 C_i}{dy^2} + \frac{2}{y} \frac{dC_i}{dy} = -\frac{1}{D_{ie}} \sum_{j=1}^{6} \sigma_{ij} r_j \rho \tag{16}$$

Catalyst energy balance equation on dehydrogenation side:

$$\frac{d^2 T}{dy^2} + \frac{2}{y} \frac{dT}{dy} = \frac{1}{k_e} \sum_{j=1}^{6} [\Delta H(T)]_j r_j \rho \tag{17}$$

Catalyst mole balance equation on hydrogenation side:

$$\frac{d^2 C'_i}{dy'^2} + \frac{2}{y'} \frac{dC'_i}{dy'} = -\frac{\sigma'_i r' \rho'}{D'_{ie}} \tag{18}$$

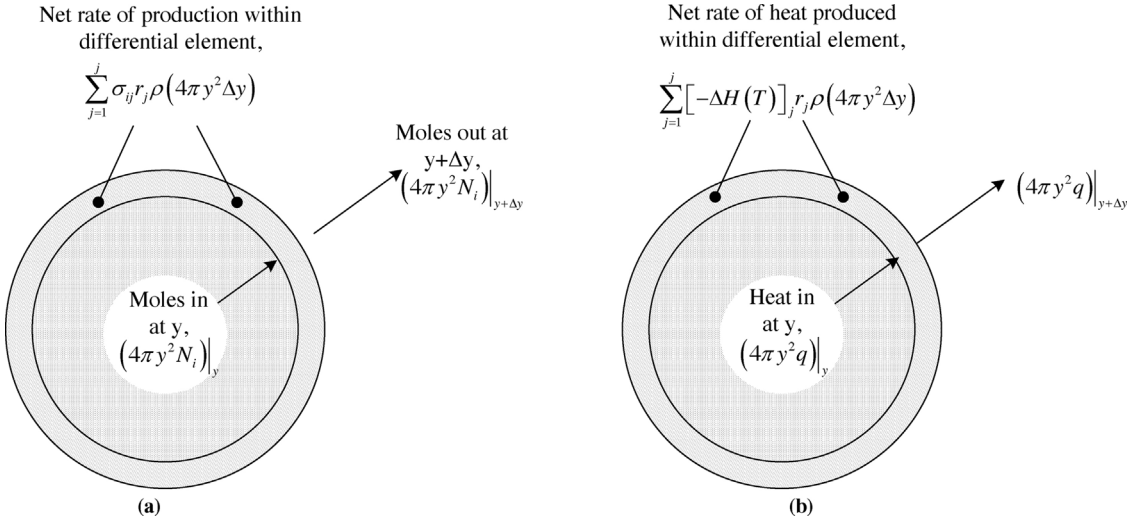

Fig. 2. Infinitesimal slice inside catalyst pellets on dehydrogenation side showing terms considered in: (a) mole balance, and (b) energy balance.

Catalyst energy balance equation on hydrogenation side:

$$\frac{d^2T'}{dy'^2} + \frac{2}{y'}\frac{dT'}{dy'} = \frac{[\Delta H(T)]' r' \rho'}{k'_e} \tag{19}$$

These coupled equations form a split boundary value problem describing the molar and energy flow inside the catalyst on both the dehydrogenation and hydrogenation sides. The boundary conditions are:

- Dehydrogenation side:

$$y = 0 \Rightarrow \begin{cases} \dfrac{dC_i}{dy} = 0 \\ \dfrac{dT}{dy} = 0 \end{cases} \tag{20}$$

$$y = R_p \Rightarrow \begin{cases} C_i = C_{is} \\ T = T_s \end{cases} \tag{21}$$

- Hydrogenation side:

$$y' = 0 \Rightarrow \begin{cases} \dfrac{dC'_i}{dy'} = 0 \\ \dfrac{dT'}{dy'} = 0 \end{cases} \tag{22}$$

$$y' = R'_p \Rightarrow \begin{cases} C'_i = C'_{is} \\ T' = T'_s \end{cases} \tag{23}$$

The effective diffusivities, i.e. D_{ie} and D'_{ie}, of component i in Eqs. (16) and (18) are calculated considering both the effective binary diffusivity of component i in a mixture D^e_{im} and the effective Knudsen diffusivity D^e_{ik} [18,19]:

$$\frac{1}{D_{ie}} = \frac{1}{D^e_{im}} + \frac{1}{D^e_{ik}} \tag{24}$$

The binary diffusivity of component i in the above equation is estimated on the dehydrogenation side from the well-known Wilke equation [18,19]:

$$\frac{1}{D_{im}} = \frac{1}{1 - x_i} \sum_{\substack{j=1 \\ j \neq i}}^{10} \frac{x_i}{D_{ij}} \tag{25}$$

The effective diffusivities are obtained [18] from:

$$D^e_{im} = \frac{\varepsilon}{\tau} D_{im} \tag{26}$$

where ε is the internal porosity of the catalyst pellet and τ is the tortuosity, and both are assumed to be isotropic properties.

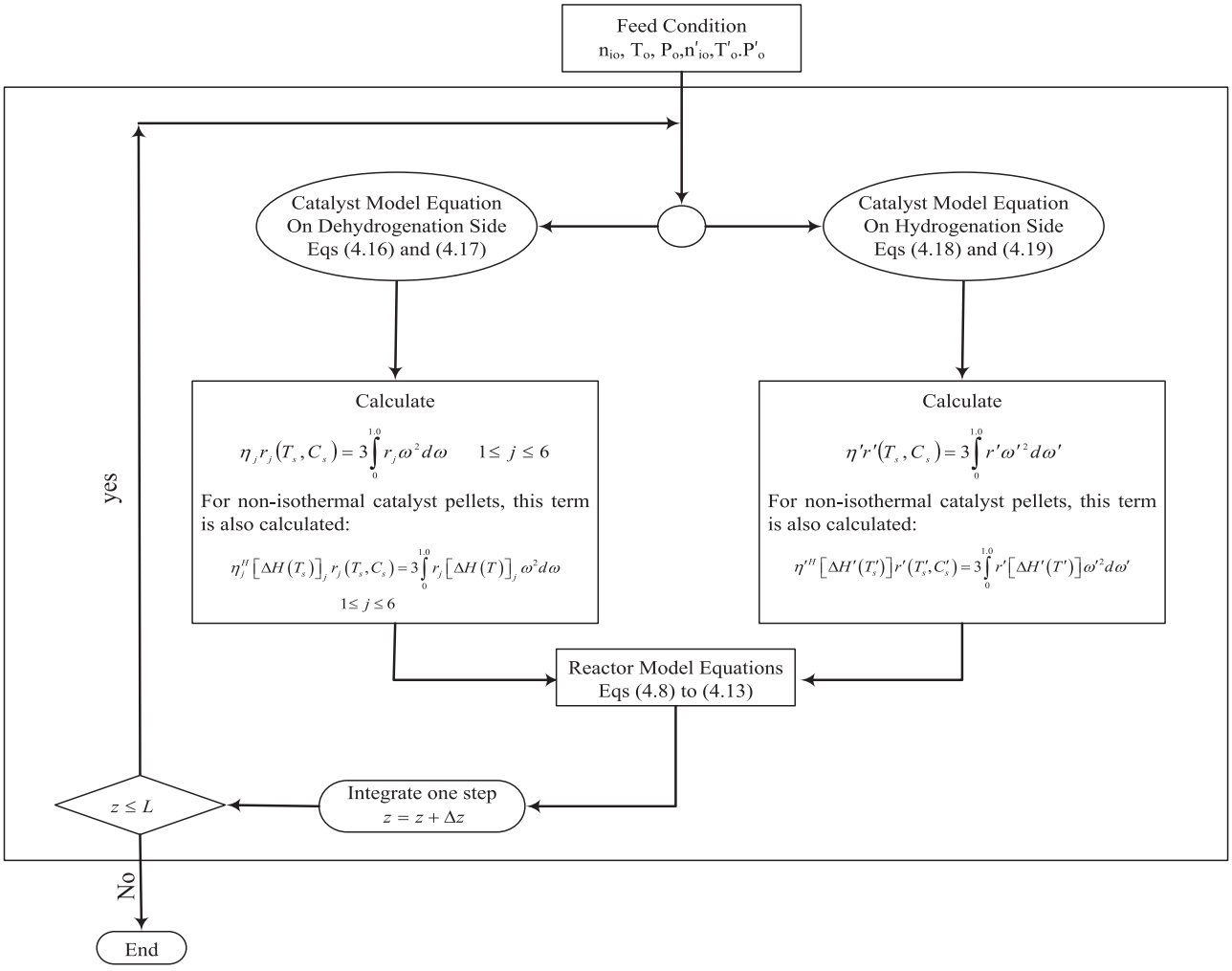

Fig. 3. Schematic sequence of computations for the catalyst and reactor models.

The numerical solution of model Eqs. (16)–(19) evaluates the average reaction rates, as well as the average heat released or absorbed due to reactions. Those values can be related to the reaction rates and heat released or absorbed at bulk conditions, i.e. concentrations and temperature, through the concept of *effectiveness factors*, defined for chemical reactions as the ratio of the rate of reaction with pore resistance to the rate of reaction evaluated at the surface conditions:

$$\eta_j = \frac{\int_0^{R_p} r_j \rho (4\pi y^2) dy}{r_j \rho (4/3\pi R_p^3)} \tag{27}$$

with $1 \le j \le 6$ for dehydrogenation side and $j = 1$ for hydrogenation side. When the dimensionless catalyst radius ($\omega = y/R_p$) is introduced into Eq. (27), the volume-averaged reaction rate can be formulated as:

$$\eta_j r_j(T_s, C_{is}) = 3 \int_0^{1.0} r_j \omega^2 d\omega \tag{28}$$

For non-isothermal catalyst pellets, a thermal effectiveness factor, relating the actual heat released or absorbed to that at the surface conditions, can be defined as:

$$\eta_j^H [-\Delta H(T_s)] r_j(T_s, C_{is}) = 3 \int_0^{1.0} r_j [-\Delta H(T)] \omega^2 d\omega \tag{29}$$

Component effectiveness factors can be defined as:

$$\eta_i = \frac{\sum_{j=1}^{j} \sigma_{ij} \int_0^{R_p} r_j \rho (4\pi y^2) dy}{\sum_{j=1}^{j} \sigma_{ij} r_j(T_s, C_{is}) \rho (4/3\pi R_p^3)} \tag{30}$$

with $1 \le j \le 6$ for the dehydrogenation side and $j = 1$ for the hydrogenation side. Integral terms in Eqs. (27)–(30) are evaluated here by the *trapezoidal rule*. Eqs. (28) and (29), representing the actual reaction rate and heat released or absorbed, are used to update reactor model Eqs. (8)–(13) in Table 3.

The conversions of ethylbenzene and nitrobenzene on both sides of the membrane reactor and component yields on the dehydrogenation side are defined as:

$$\text{Conversions} \begin{cases} X_{EB} = \dfrac{n_{EBo} - n_{EB}}{n_{EBo}} & \text{on Dehydrogenation Side} \\ X_{NB} = \dfrac{n_{NBo} - n_{NB}}{n_{NBo}} & \text{on Hydrogenation Side} \end{cases} \tag{31}$$

$$\text{Yields} \begin{cases} Y_{ST} = \dfrac{n_{ST} - n_{STo}}{n_{EBo}} \\ Y_{BZ} = \dfrac{n_{BZ} - n_{BZo}}{n_{EBo}} \\ Y_{TO} = \dfrac{n_{TO} - n_{TOo}}{n_{EBo}} \end{cases} \tag{32}$$

The sequence of computations followed to link the reactor model equations with the catalyst pellets model equations is shown schematically in Fig. 3. The sequence starts by using the bulk conditions to establish the boundary conditions to solve the catalyst model Eqs. (16) and (17) on the dehydrogenation side and (18) and (19) on the hydrogenation side. These numerical solutions are then used to evaluate the molar and heat flux at the surface of the catalyst numerically by evaluating Eqs. (28) and (29), substituted in the reactor model equations, i.e. (8)–(13), which can then be integrated one step forward. To compute exchange of hydrogen and heat between the hydrogenation and dehydrogenation side, Eqs. (14) and (15) are used. This procedure is repeated until the entire length of the reactor is covered. Hence, the complete model consists of Eqs. (8)–(19) and (28) and (29). Solving these equations as mentioned above results in the simulations presented.

Table 4
Dimensional and operating parameters for hybrid catalytic membrane reactor for base case.

Parameter	Value	Units
Dimensional variables		
Net diameter of the dehydrogenation side	1.95	m
Diameter of the hydrogenation tube	3.5×10^{-2}	m
Total number of the hydrogenation tubes	1500	–
Length of the reactor	4.0	m
Operating conditions (dehydrogenation side)		
Ethylbenzene	10.242	mol/s
Styrene	0.1861	mol/s
Benzene	0.0306	mol/s
Toluene	0.2444	mol/s
Steam	125.86	mol/s
Temperature	880.0	K
Pressure	2.5	bar
Catalyst density	2146.3	kg/m^3
Catalyst thermal conductivity	0.3	J/m/s
Pore diameters	4800×10^{-10}	m
Catalyst porosity	0.35	–
Catalyst tortuosity	4.0	–
Bed voidage	0.48	–
Operating conditions per one tube (hydrogenation side)		
Nitrobenzene	0.003	mol/s
Steam	0.008	mol/s
Temperature	900.0	K
Pressure	1.0	bar
Catalyst density	1400	kg/m^3
Catalyst thermal conductivity	0.05	J/m/s
Pore diameters	5000×10^{-10}	m
Catalyst porosity	0.40	–
Catalyst tortuosity	4.0	–
Bed voidage	0.46	–

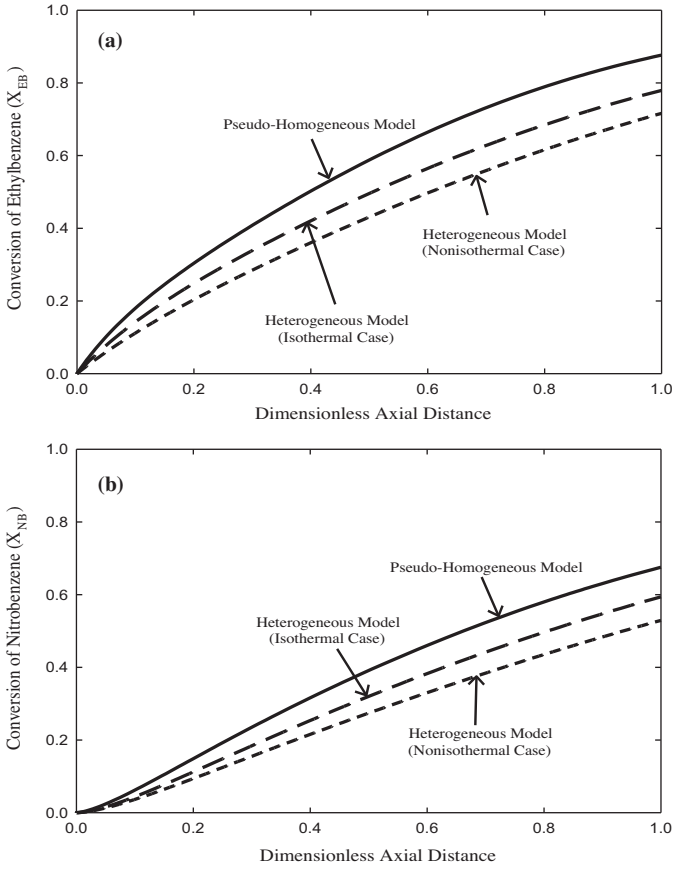

Fig. 4. Conversion of key components: (a) ethylbenzene on dehydrogenation side, and (b) nitrobenzene on hydrogenation side.

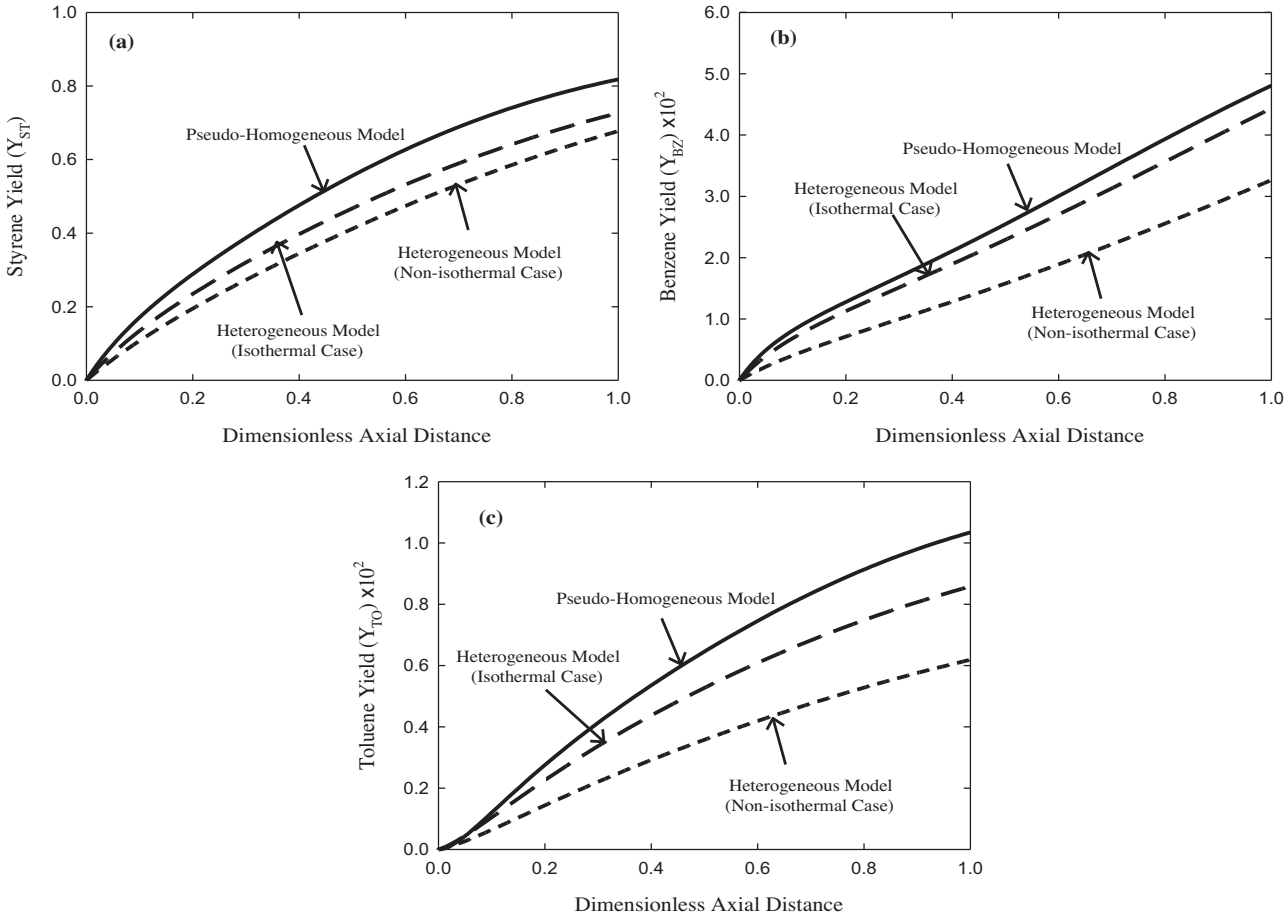

Fig. 5. Yield of: (a) styrene, (b) benzene, and (c) toluene on dehydrogenation side.

In this computational sequence, two Matlab® (The MathWorks, Natick) subroutines are invoked. The catalyst model equations are solved by bvp4c, with a relative tolerance of 1×10^{-4}, while the reactor model equations are integrated by ode15s, with a relative tolerance of 1×10^{-8}.

4. Results and discussion

This section presents and discusses the numerical results when the model developed in the previous sections is employed. The effect of the intraparticle diffusion on the performance of the catalytic membrane reactor coupling dehydrogenation of ethylbenzene with hydrogenation of nitrobenzene to aniline was simulated for the operating conditions listed in Table 4. The component molar flow rates and feed pressure on the dehydrogenation side are based on industrial fixed bed reactors. A feed temperature difference of 20 K is chosen to ensure that heat always transfers in the right direction from the hydrogenation to the dehydrogenation side.

In the following sub-sections, the predictions of several reactor variables are compared and discussed based on three models, i.e. (*i*) homogeneous model, (*ii*) heterogeneous model with isothermal catalyst pellets, and (*iii*) heterogeneous model with non-isothermal catalyst pellets. For the homogeneous model, the effect of diffusional intrusion was neglected and the reaction rates were evaluated at the bulk conditions on both sides of the reactor. For the heterogeneous reactor model with isothermal catalyst pellets, however, the diffusional model Eqs. (16) and (18) were solved to evaluate the actual reaction rates and net heat liberated due to reactions from Eqs. (28) and (29). In the heterogeneous model with nonisothermal catalyst pellets, Eqs. (16) and (17) on the dehydrogenation side and (18) and (19) on the hydrogenation side were considered to evaluate the actual reaction rate and heat due to reactions on both sides of the reactor using again Eqs. (28) and (29).

4.1. Conversion of ethylbenzene and nitrobenzene

The conversion of (*i*) ethylbenzene on the dehydrogenation side and of (*ii*) nitrobenzene on the hydrogenation side are plotted versus the dimensionless distance along the reactor in Fig. 4a and b for the homogeneous and heterogeneous model with isothermal and non-isothermal catalyst pellets. In Fig. 4a, the conversion of ethylbenzene on the dehydrogenation side of the catalytic membrane reactor increases monotonically along the catalytic membrane reactor due to the consumption of ethylbenzene. For the selected operating and design conditions, the homogeneous model predicts an ethylbenzene conversion of ~88%. When the effect of intraparticle diffusion is included, the ethylbenzene conversion predicted by the heterogeneous model is significantly lower, ~78% for isothermal pellets and ~71% for non-isothermal pellets.

Conversion of nitrobenzene on the hydrogenation side of the catalytic membrane reactor in Fig. 4b shows similar behavior to that of ethylbenzene, i.e. it increases monotonically along the reactor. It is predicted to reach ~68% by the homogenous model, ~59% by the heterogeneous model for isothermal catalyst pellets, and ~52% by the heterogeneous model for non-isothermal pellets.

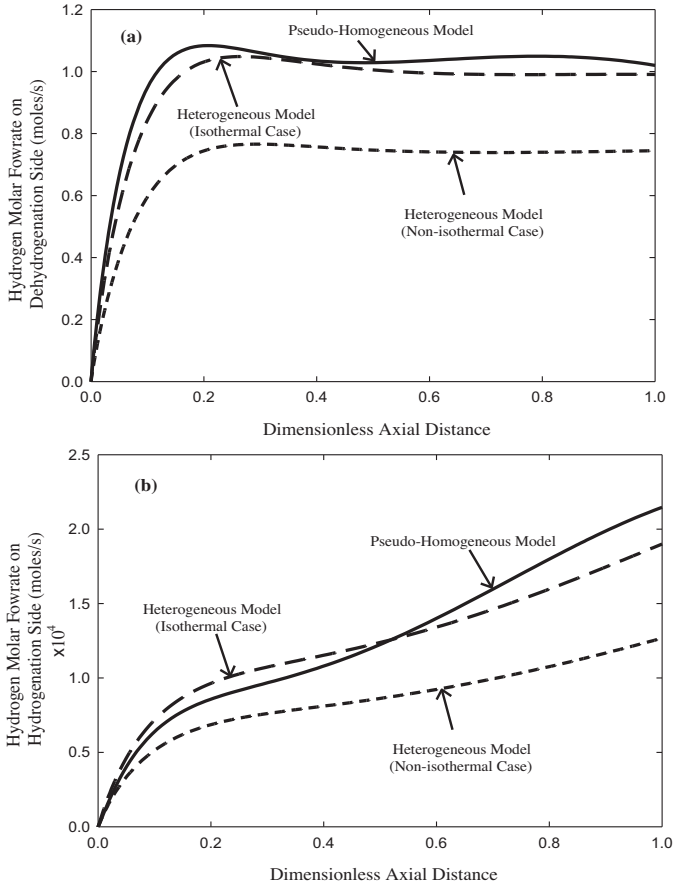

Fig. 6. Hydrogen molar flowrates on: (a) dehydrogenation side, and (b) hydrogenation side.

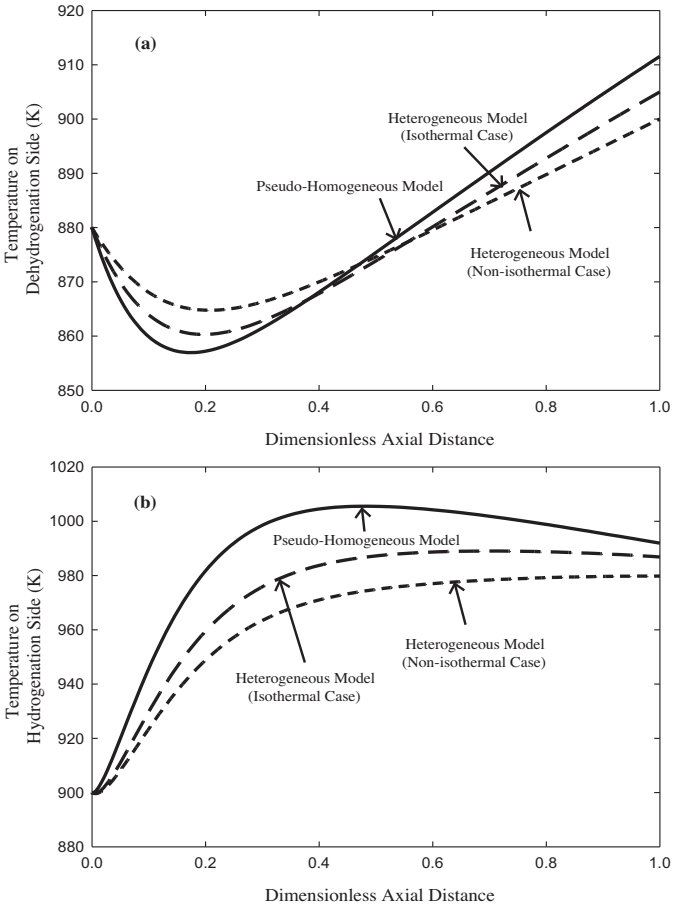

Fig. 7. Temperature profiles on: (a) dehydrogenation side, and (b) hydrogenation.

4.2. Yield of styrene, benzene, and toluene on dehydrogenation side

Fig. 5a–c, plot the yields of styrene, benzene, and toluene versus the dimensionless axial distance along the reactor. All three yields increase along the reactor, with appreciable differences in prediction among the models. The homogeneous model for the catalytic membrane reactor predicts a styrene yield of ~82%, a benzene yield of ~5.0%, and a toluene yield of ~1.0%. The heterogeneous model, on the other hand, predicts a styrene yield of ~73%, a benzene yield of ~4.6%, and a toluene yield of ~0.8% for isothermal catalyst pellets while it predicts corresponding yields of ~69%, ~3.2% and ~0.6% for non-isothermal pellets.

4.3. Hydrogen molar flow rates on the dehydrogenation and hydrogenation sides

The molar flow rates of hydrogen on both sides of the catalytic membrane reactor are plotted versus the dimensionless axial distance in Fig. 6a and b. As shown in Fig. 6a, the hydrogen molar flow rate on the dehydrogenation side predicted by both homogenous and heterogeneous models increases monotonically in the first portion of the reactor fraction length until it reaches a maximum where the rate of hydrogen diffusion to the hydrogenation side is balanced by the hydrogen net production due to the reactions. After that, the hydrogen molar flow rate continues at a nearly constant level to the reactor exit. The hydrogen flow rate predicted by the heterogeneous model for the non-isothermal catalyst pellets is significantly lower than that predicted by either the homogenous model or the heterogeneous model with isothermal catalyst pellets, due to the significant effect of temperature. This gives a strong indication of the significance of intraparticle heat resistance in retarding the chemical reactions and the diffusion through the membranes.

The molar flow rate of the diffused hydrogen toward the hydrogenation tubes is plotted in Fig. 6b as a function of the dimensionless axial distance. All three models predict monotonically increasing profiles, with a significant difference for the heterogeneous model with non-isothermal catalyst pellets. At the reactor entrance, the homogenous model and the heterogeneous model for the isothermal catalyst pellets give similar predictions over 40% of the reactor length, with a somewhat higher subsequent value for the heterogeneous model with isothermal catalyst pellets, resulting from a higher hydrogen diffusion rate compared to that predicted by the homogenous model. The difference in the predictions of these two models becomes more pronounced as the reactor exit is approached. The prediction of the heterogeneous model for the non-isothermal case is considerably lower than for the other two models due to the temperature gradient inside the catalyst pellets.

4.4. Temperature profiles along coupled reactor

Temperature profiles along the reactor on both the shell and tube sides are plotted in Fig. 7a and b. In Fig. 7a, the temperature on the dehydrogenation side decreases over the first 15% of the reactor length due to the net endothermic heat of the reaction. A point is then reached where the heat lost is balanced by the heat gained from the hydrogenation side. Given the large temperature difference established between the two sides of the integrated reactor, the temperature on the shell side then increases over the reminder

of the reactor due to significant heat transfer from the tube side. The temperature profiles predicted by all three models are similar in shape.

In Fig. 7b, the temperature profiles predicted by the three models, are plotted against dimensionless axial distance along the reactor. The temperature on the hydrogenation side rises due to the high exothermic heat of reaction. A clear maximum temperature is obtained from the homogenous model about 40% of the way along the reactor at which the heat transferred to the dehydrogenation side balances the endothermic requirement of the main reaction. This point is clearly observable for the homogeneous model, while it is less observable in the profiles predicted by the heterogeneous model for isothermal catalyst pellets, and not observable for the heterogeneous model with non-isothermal catalyst pellets.

From the temperature profiles on both sides of the reactor, it should be noted that the intraparticle diffusion resistance not only retards the chemical reactions, but also the heat transfer between the two sides by reducing the driving force, i.e. the temperature difference between the dehydrogenation and hydrogenation compartments.

4.5. Reaction effectiveness factors and reaction rates

Intraparticle effectiveness factors, defined as the ratios of the observed rates of reaction to those evaluated if the surface conditions prevailed throughout the catalyst pellets, are plotted versus the bulk temperature in Fig. 8 for both sides of the membrane. Actual reaction rates and those evaluated at the conditions of the catalyst surface are plotted in Fig. 9. In Fig. 8a, effectiveness factors for both reactions (1) and (2) exhibit a strong nonlinear behavior with different turning points. The bulk temperatures at which the turns take place correspond to the axial location inside the reactor at which the net endothermic heat of reactions balances the heat transferred from the hydrogenation side. While the effectiveness factors of reactions (1) and (2) for the isothermal case are slightly lower than 1.0, those for the non-isothermal case are significantly lower, indicating the significance of the intraparticle heat resistance. Consequently, the difference between the actual reaction rates and these evaluated at the conditions of the catalyst pellet surface for reactions (1) and (2) is higher for the non-isothermal case than for the isothermal catalyst pellets, as shown in Fig. 9. As the bulk temperature increases, the actual reaction rates for both the isothermal and non-isothermal cases and those evaluated at the surface conditions approach each other. The actual rate of reaction (1) for the isothermal case coincides with that for the non-isothermal case when the bulk temperature on the dehydrogenation side exceeds 865 K.

The effectiveness factors of the other reactions, i.e. reaction (3)–(6), for the isothermal and non-isothermal catalyst pellets, plotted in Fig. 8b also exhibit highly nonlinear behavior with different turning points. Their values start from infinity, decrease sharply in the first part of the reactor, then turn around and decrease as the bulk temperature increases until they fall below unity. The initial infinite values of the effectiveness factors result from the fact that the reaction rates at the surface of the catalyst start at zero due to the absence of some components in the bulk such as hydrogen. In Fig. 8b, all four effectiveness factors of the reactions pass through a point in the reactor where the intraparticle resistances are negligible, i.e. $\eta_3 = \eta_4 = \eta_5 = \eta_6 = 1.0$. This point can be identified in Fig. 9 by those points at which the actual reaction rates are equal to those evaluated at the surface conditions. The temperature at which this occurs varies from one reaction to another, e.g. ~860 K for reaction (3), ~861 K for reaction (4), ~875 K for reaction (5), and ~864 K for reaction (6) for isothermal pellets and ~873 K for reaction (3), ~874 K for reaction (4), ~870 K for reaction (5), and ~868 K for reaction (6) for non-isothermal pellets. The large

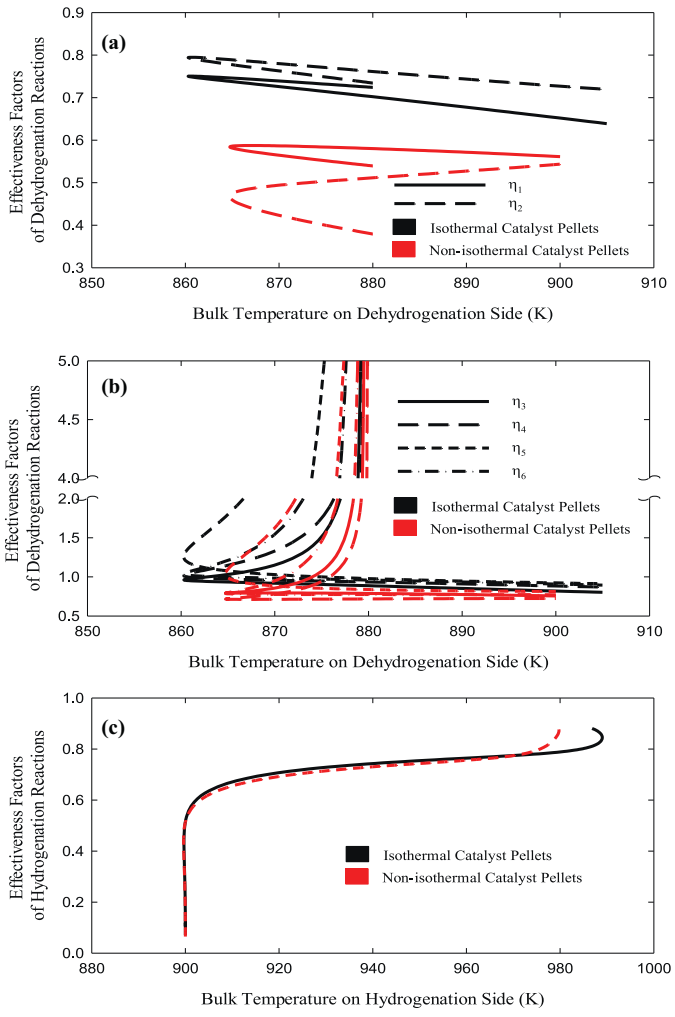

Fig. 8. Reaction effectiveness factor profiles versus bulk temperature for: (a and b) dehydrogenation reactions, and (c) hydrogenation reaction.

effectiveness factor in Fig. 8b indicates the large differences between the actual reaction rates and those evaluated at the catalyst surface, with the consequence that the homogenous model predictions must be interpreted with care, e.g. when utilized in optimization studies.

On the tube side, the hydrogenation reaction rate is zero at the entrance of the reactor as shown in Fig. 9 due to the absence of hydrogen in the feed stream. Due to the diffusion of hydrogen from the dehydrogenation side to the hydrogenation side, the intraparticle effectiveness factor increases sharply from $\eta \ll 1.0$ to ~0.7. The hydrogenation effectiveness factors for isothermal and non-isothermal catalyst pellets in Fig. 8c vary in a nonlinear manner with the bulk temperature. The effectiveness factors for both isothermal and non-isothermal cases are almost identical for temperatures on the hydrogenation side lower than 970 K. Similar behavior is shown in Fig. 9, with a constant difference between the actual reaction rates and those evaluated at the condition of the surface of the catalyst pellets. For temperatures exceeding 970 K, the effectiveness factors for both cases diverge, approaching unity as shown in Figs. 8c and 9, with the actual reaction rates and those evaluated at the surface approach each other.

4.6. Component effectiveness factors

The component effectiveness factors defined by Eq. (30) are the ratios of the actual net production rates of component i to those

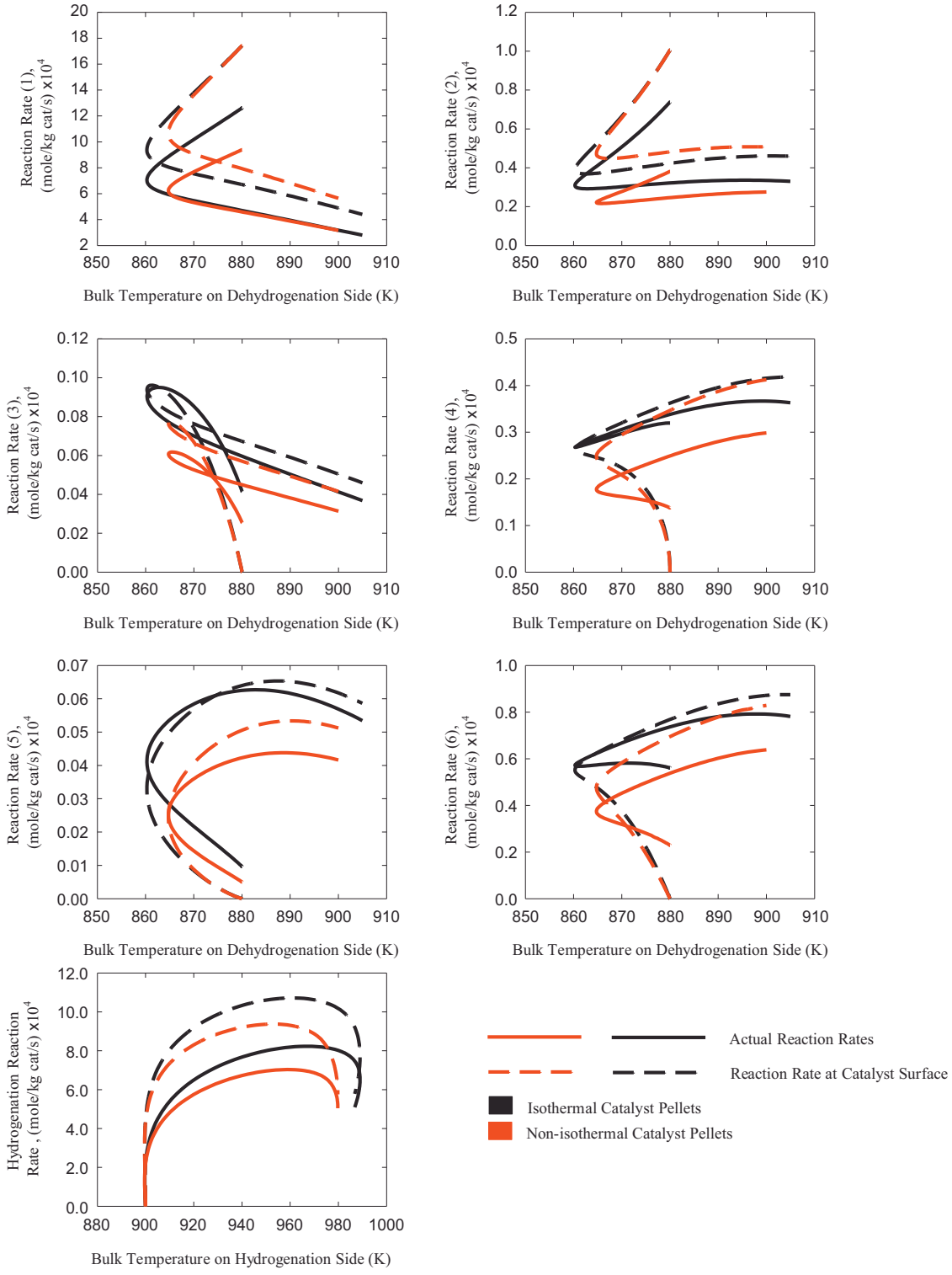

Fig. 9. Actual reaction rates and their values at surface conditions versus bulk temperature for all reactions.

evaluated for the surface conditions of the catalyst pellets. In Fig. 10, they are plotted for key species i.e. ethylbenzene, styrene, hydrogen, benzene, toluene and nitrobenzene for the heterogeneous model with both isothermal and non-isothermal catalyst pellets. On the dehydrogenation side, the component effectiveness factors show a non-monotonic behavior when plotted against the dimensionless axial distance along the reactor for all components except toluene for both isothermal and non-isothermal catalyst pellets. The toluene effectiveness factor is infinite at the inlet of the reactor because components involved in the production reaction diffuse to the active sites of the catalyst and react. It then decreases with increasing distance along the reactor, passing a point where the actual rate of production reaction is equal to the reaction rate at the surface conditions ($\eta_{TO} = 1.0$) as hydrogen is produced on the dehydrogenation side and the surface reaction rate becomes significant, finally it approaches $\eta_{TO} = 0.80$. As hydrogen is produced

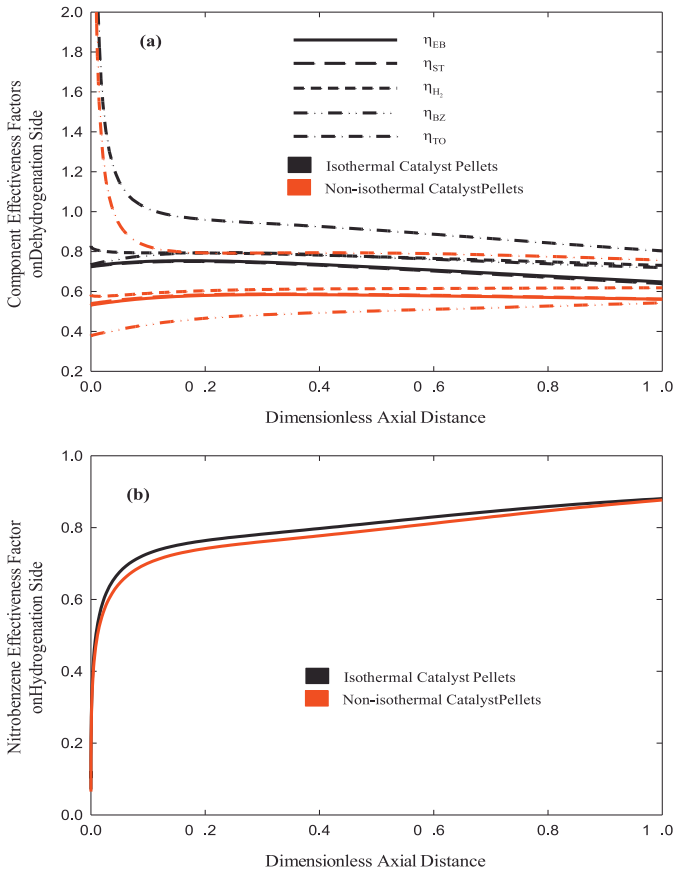

Fig. 10. Component effectiveness factor profiles versus dimensionless axial distance for: (a) ethylbenzene, styrene, hydrogen, benzene, and toluene on dehydrogenation side; and (b) nitrobenzene on hydrogenation side.

in the bulk, the toluene effectiveness factor drops sharply. In general, the component effectiveness factors reflect the fact that the net production rates of the components from the homogeneous model are not as accurate as from the heterogeneous models.

The nitrobenzene effectiveness factors on the hydrogenation side for both isothermal and non-isothermal catalyst pellets plotted in Fig. 10b behave in a similar manner. They are mathematically undefined at the inlet point of the rector, due to the absence of hydrogen in the compartment, making both the diffusion to the catalyst active sites as well as reaction at the surface zero. As hydrogen diffuses to the hydrogenation compartment though the membrane, a sharp increase is observed in both effectiveness factors, heading toward 1.0. Note that the differences between both factors for isothermal and non-isothermal catalyst pellets are negligible.

4.7. Behavior inside the catalyst pellets on both sides of the coupled reactor

In Fig. 11, the intraparticle mole fractions, temperature and component effective diffusivity profiles on the dehydrogenation side are plotted at three axial positions, i.e. $z/L = 0.1$, 0.5, and 0.8. The abscissa in Fig. 11 is interpreted as the dimensionless radial distance inside the catalyst pellet, i.e. $\omega = 0.0$ represents the center of the catalyst pellet, while $\omega = 1.0$ indicates its surface.

As can be seen, the ethylbenzene mole fraction at the pellet surface decreases as the fractional length increases from 0.1 (close to the inlet of the reactor) to 0.8 (close to the exit) due to the consumption in the bulk. Although the profiles for the other components are not presented for brevity, it has been observed that the production of these, i.e. hydrogen, benzene, and toluene, are limited. The mole

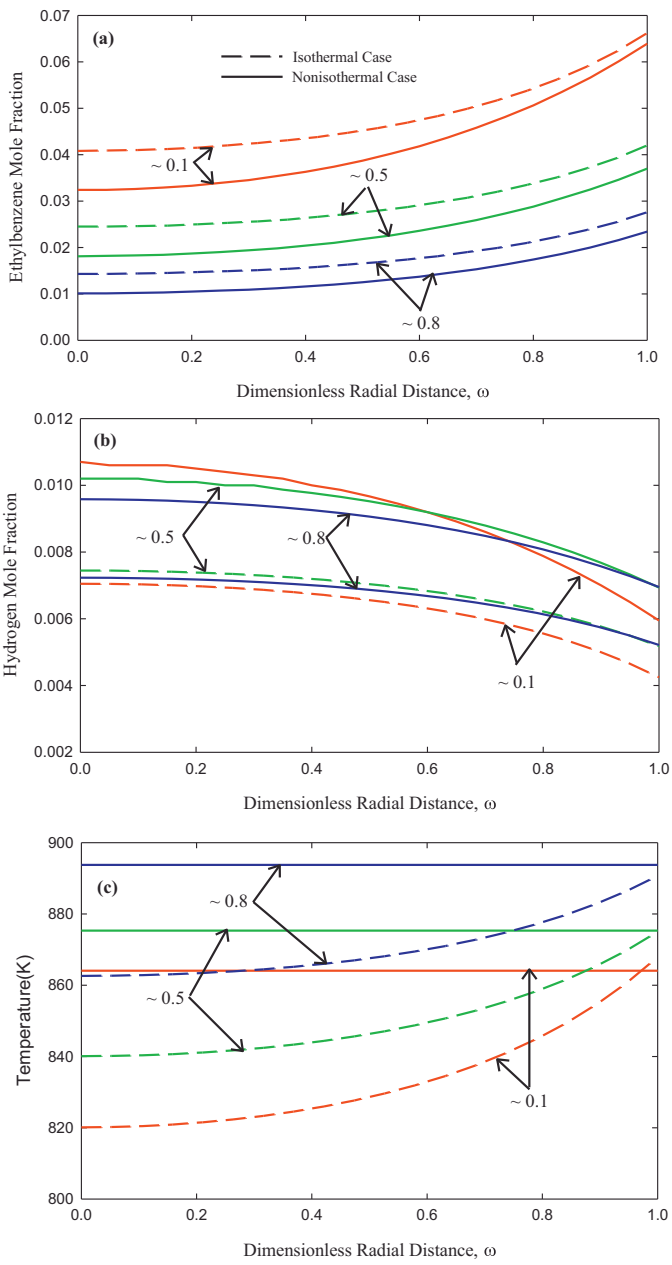

Fig. 11. Intraparticle profiles of ethylbenzene and hydrogen mole fractions, and temperature at fractional lengths of 0.1, 0.5, and 0.80 for both the isothermal and non-isothermal catalyst pellet cases on dehydrogenation side.

fraction of hydrogen on the surface of the catalyst pellet is less than 0.01 due to diffusion through the membrane to the hydrogenation side.

The thermal resistance inside the catalyst pellet is detrimental as it reduces the production of all components inside the catalyst particles. The drop in temperature inside the catalyst pellet decreases from ~50 K at $z/L = 0.1$ to ~25 K at $z/L = 0.8$. This is because at the inlet of the reactor, the mole fractions of the reactants are high at the catalyst surface, while this is no longer the case when the reactor exit is approached.

Hydrogen has the highest effective diffusivities inside the catalyst pellet because of its small molecular size. As a consequence for the heat transferred from the tube side to the shell side, the diffusivities increase with the distance along the reactor. Inside the catalyst, however, hydrogen diffusivity decreases as the center of the particle is approached due to the drop in temperature.

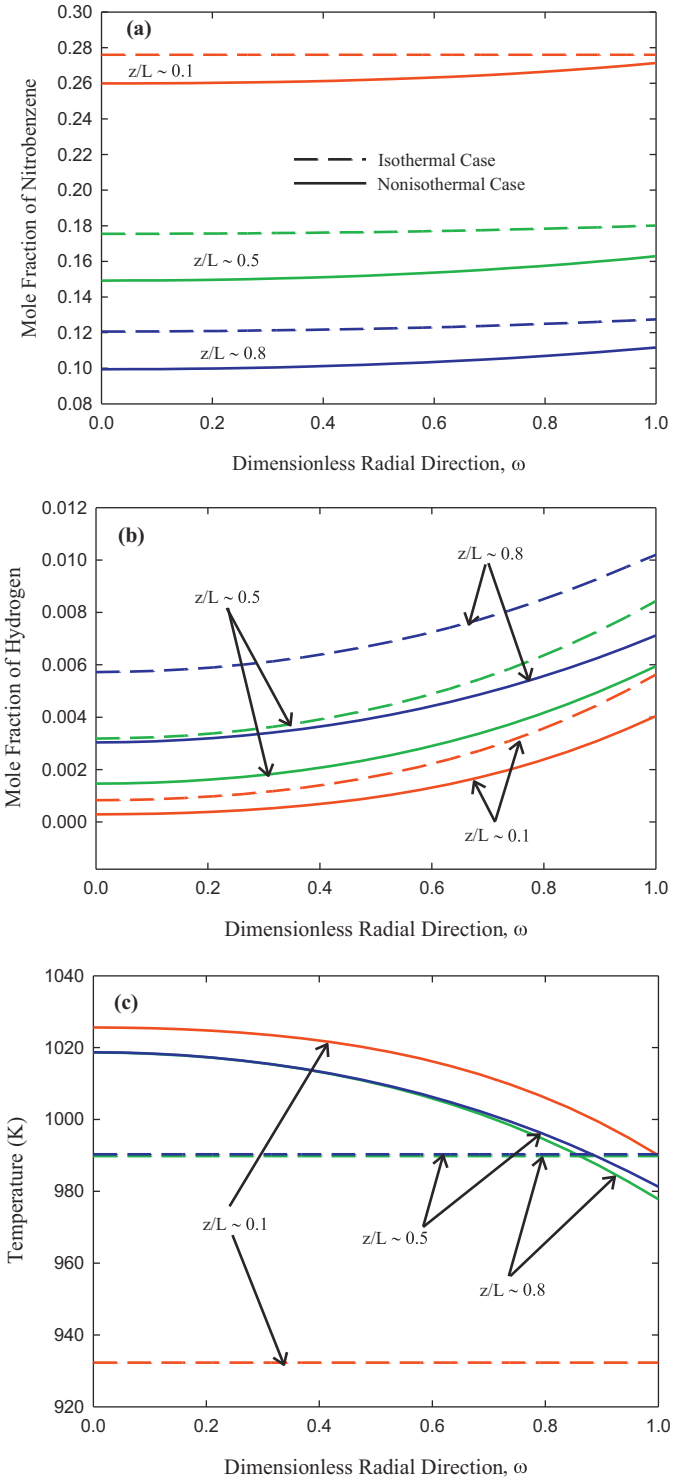

Fig. 12. Intraparticle profiles of nitrobenzene and hydrogen mole fractions, and temperature at fractional lengths of 0.1, 0.5, and 0.80 for both the isothermal and non-isothermal catalyst pellet cases on hydrogenation side.

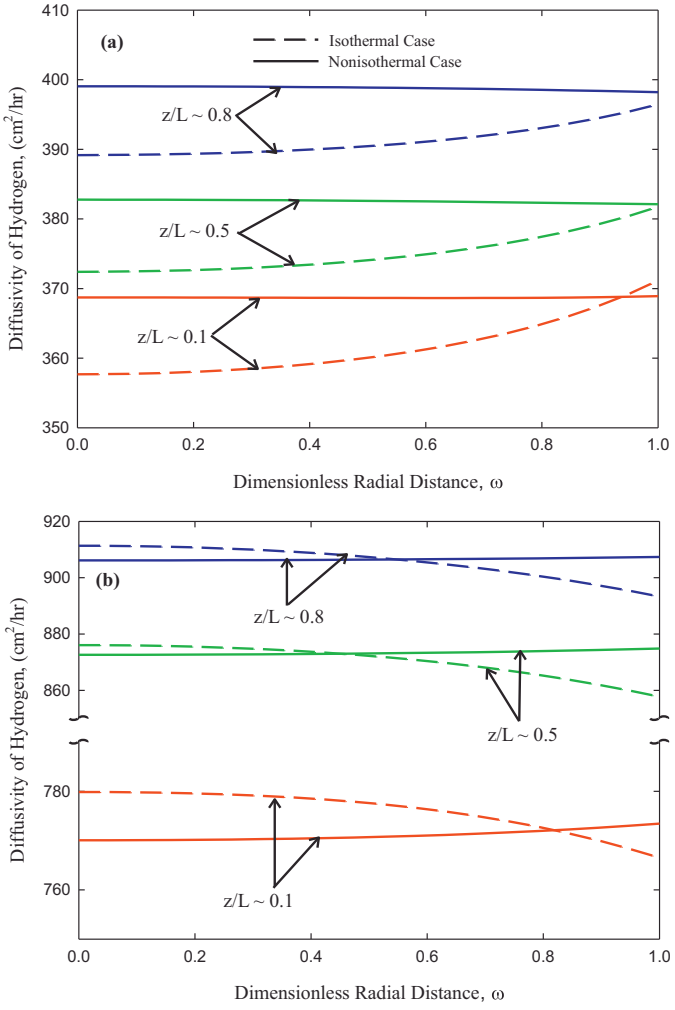

Fig. 13. Effective diffusivity of hydrogen inside the catalyst pellet on both sides of the reactor at fractional lengths of 0.10, 0.50, and 0.80 for both the isothermal and non-isothermal catalyst pellet cases.

The effect of temperature on the component effective diffusivities is greater than that of compositions when both isothermal and non-isothermal profiles are compared. The effective diffusivities of the other components, i.e. ethylbenzene, styrene, benzene and toluene, are limited within the range from 44 to 53 cm^2/h. The effective diffusivity of ethylbenzene decreases as the outlet of the reactor is approached as a result for the decrease of ethylbenzene concentration in the bulk phase. Similar behavior is also observed inside the catalyst pellet, but this decrease becomes more pronounced as the temperature inside the catalyst pellets drops. The effective diffusivities of styrene, benzene and toluene increase at the surface of the catalyst pellets as the outlet of the reactor is approached due to their production in the bulk, and the increase in temperature, due to the heat transfer, whereas they decrease inside the catalyst as the center is approached, due to the drop in temperature which has a more pronounced effect than variation in mole fractions.

On the hydrogenation side, the mole fraction of nitrobenzene decreases at the surface of the catalyst as the fractional length increases from 0.1 to 0.8 and also as the center of the catalyst pellet is approached as shown in Fig. 12. This drop in mole fraction is more significant for the isothermal catalyst pellets than for the non-isothermal catalyst pellets. Aniline, on the other hand, exhibits the opposite behavior; it increases at the surface of the catalyst and inside the catalyst pellets with increasing distance along the reactor and decreasing radius inside the catalyst pellet.

The temperature profile, on the other hand, decreases at the surface of the catalyst as the fraction length increases, i.e. it is ~990 K at $z/L = 0.1$ and ~980 K at $z/L = 0.8$. This decrease is due to the transfer of heat from the hydrogenation side to the dehydrogenation side. The rise in the temperature inside the catalyst pellet is ~35 K, and this is maintained as the exit of the reactor is approached.

As far as the effective component diffusivities are concerned, it is observed in Fig. 13 that hydrogen maintains the same performance

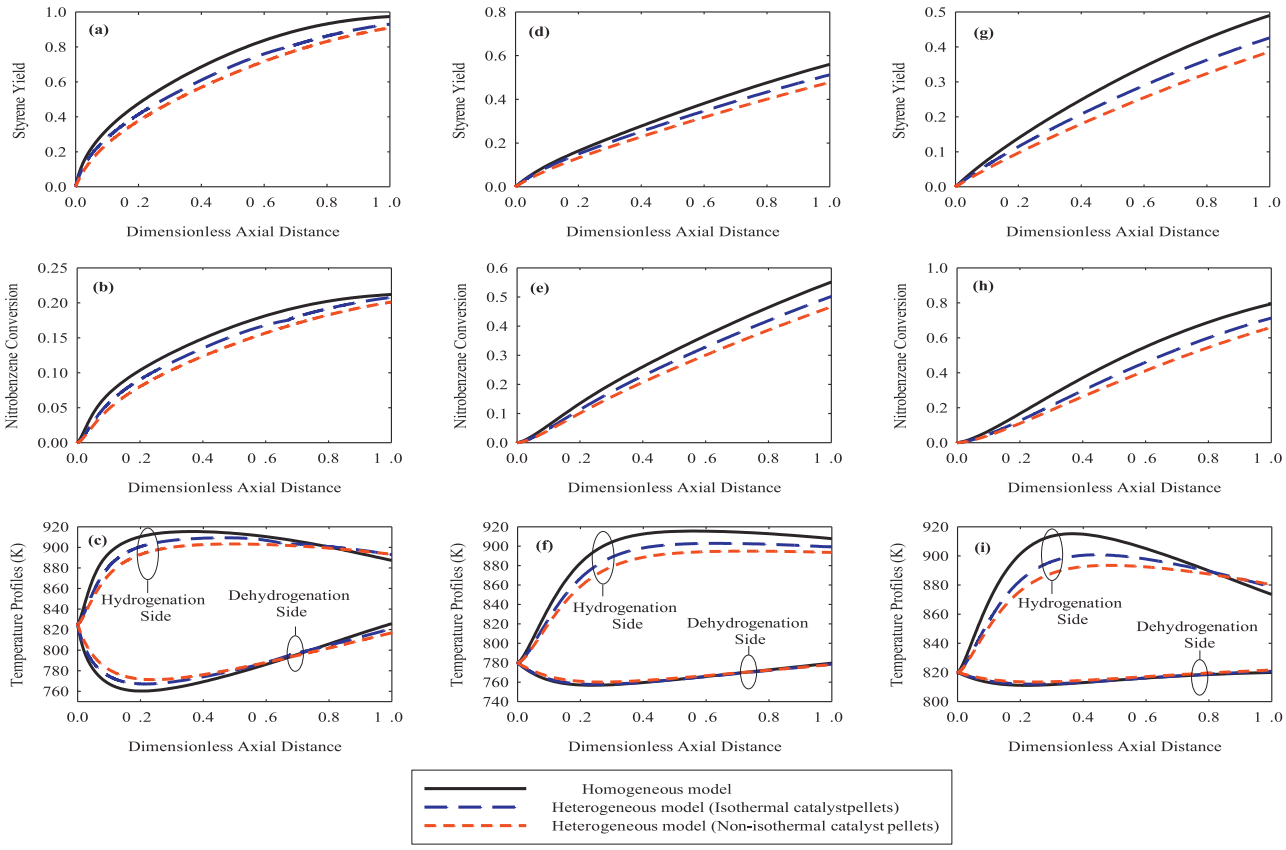

Fig. 14. Styrene yield, nitrobenzene conversion, and temperature profiles for the optimal designs of the coupled membrane reactor, i.e. *solution A* (a–c), solution *B* (d–f), solution *C* (g–i).

due to its highest effective diffusivity. An increase in the effective diffusivities of most components is also observed as the dimensionless radial distance ω goes to 0 when the profiles of isothermal catalyst pellets, are compared to those for non-isothermal pellets although they have not been shown for brevity. For nitrobenzene, the effective diffusivities decrease slightly at the surface of the catalyst and inside the catalyst as a result of being consumed in the bulk and inside the catalyst. Aniline effective diffusivities, however, increase at the surface of the catalyst pellets as the exit of the reactor is approached and inside the catalyst pellets as the center is approached due to its production in the bulk, as well as inside the catalyst. The temperature rise for the non-isothermal catalyst pellets also plays an important role in enhancing the diffusivities of aniline.

4.8. Effect of intraparticle diffusion resistance on the reactor optimal design

In an earlier paper [20], the authors addressed the bi-objective optimization problem of this coupled membrane reactor. The two objective functions considered were: (*i*) the *yield of styrene* on the dehydrogenation side, and (*ii*) the *conversion of nitrobenzene* on the hydrogenation side. The homogenous reactor model was used for the calculations. 12 operating and design parameters were used to optimize the objectives considering a number of linear and nonlinear constraints. The Pareto set, representing the set of optimal solutions, was obtained by similar approaches as in [21] using two numerical scalarisation based multi-objective techniques: the normalized normal constrained method and the normal boundary intersection method. In this optimization problem, the production of styrene on the dehydrogenation side can be increased by maximizing the yield of styrene, whereas the production of aniline can be increased on the hydrogenation side by maximizing the conversion of nitrobenzene. Optimal solutions are summarized in Table 5 representing three cases where the focus is on: (*i*) production of styrene only (*solution A*), (*ii*) production of both styrene and aniline (*solution B*), and (*iii*) production of aniline only (*solution C*).

Testing the heterogeneous reactor model developed for the membrane reactor has revealed differences in the values of both objectives, i.e. styrene yield and nitrobenzene conversion, for all three optimal solutions. For instance, the homogenous model predicts a styrene yield of 0.975 on the dehydrogenation side for *solution A*, whereas the heterogeneous predicts 0.930 for the isothermal catalyst pellets and 0.925 for the non-isothermal pellets. On the hydrogenation side, the homogeneous model predicts a nitrobenzene conversion of 0.211, whereas the heterogeneous model predicts 0.208 for isothermal pellets and 0.202 for non-isothermal pellets. For *solution B*, the homogenous model predicts a styrene yield of 0.564 on the dehydrogenation side, whereas the heterogeneous model 0.518 for isothermal pellets and 0.488 for non-isothermal catalyst pellets. The nitrobenzene conversion predicted on the hydrogenation side is 0.555 by the homogenous model, 0.508 by the heterogeneous model for the isothermal catalyst pellets, and 0.477 by the heterogeneous model for the non-isothermal catalyst pellets. For *solution C*, the styrene yield predicted on the dehydrogenation side by the homogenous model is 0.491, 0.428 by the heterogeneous model for the isothermal pellets, and 0.396 by heterogeneous model for the non-isothermal pellets. On the hydrogenation side, the predicted nitrobenzene conversion is 0.796 from the homogenous model, 0.720 from the heterogeneous model for isothermal pellets, and 0.675 by the heterogeneous model for non-isothermal pellets. There are also significant differences in temperature profiles along both sides of the reactor. These differences may result in overestimating the design and operating parameters due

Table 5
Representative solutions for Pareto frontier.[a]

Parameter		Optimal *solution A*	Optimal *solution B*	Optimal *solution C*
Dehydrogenation side	Feed molar of ethylbenzene (mol/s)	**7.66**	9.36	**11.27**
	Steam-to-ethylbenzene ratio	**7.00**	**7.00**	**20.00**
	Feed temperature on shell side (K)	825.41	780.00	820.02
	Feed pressure on shell side (bar)	**4.00**	2.52	**4.00**
Hydrogenation side	Feed molar of nitrobenzene (mol/s)	**0.005**	**0.002**	**0.002**
	Steam-to-nitrobenzene ratio	**4.00**	**4.00**	**4.00**
	Feed temperature on tube side (K)	825.41	780.00	820.02
	Feed pressure on tube side (bar)	3.62	**1.00**	**1.00**
Dimensional variables	No. of hydrogenation tubes	**2500**	1582	**1000**
	Equivalent-area diameter of dehydrogenation side (m)	**3.00**	2.39	**1.95**
	Diameter of hydrogenation tube (m)	0.048	0.035	0.040
	Reactor length (m)	**4.00**	**4.00**	**4.00**
Yield of styrene	Homogeneous modeling	0.9747	0.5644	0.4909
	Heterogeneous modeling (isothermal catalyst pellets)	0.9300	0.5124	0.4259
	Heterogeneous modeling (non-isothermal catalyst pellets)	0.9245	0.4775	0.3859
Conversion of nitrobenzene	Homogeneous modeling	0.2119	0.5548	0.7957
	Heterogeneous modeling (isothermal catalyst pellets)	0.2078	0.5018	0.7130
	Heterogeneous modeling (non-isothermal catalyst pellets)	0.2011	0.4663	0.6594

[a] Bold values are constrained limits.

to neglecting important effects caused by the intraparticle diffusion resistance. Styrene yield, nitrobenzene conversion and temperature profiles on both sides of the reactor are plotted in Fig. 14.

In summary, the homogeneous model systematically overestimates the conversion and yield by 5–15% of their actual values. However, the computation times required for one simulation of the homogeneous model and the heterogeneous non-isothermal model are less than 4 s and around a day, respectively. Supplying the analytical Jacobians for the boundary value problems in the catalyst pellet models, as well as using vectorization options, can help significantly in reducing the execution time to around twenty minutes. Hence, as the trends are generally well-captured by the simpler homogeneous model, this one may in practice serve for a preliminary rapid screening of different alternatives, or even a first systematic optimization purpose. Nevertheless, these results must be interpreted with due care, given the model's tendency to overestimate. Afterwards, the design and optimization can be fine-tuned based on the more complex heterogeneous (non-isothermal) model.

5. Conclusion

In order to evaluate the importance of intraparticle resistances in a novel coupled membrane reactor integrating the dehydrogenation of ethylbenzene with the hydrogenation of nitrobenzene in view of process intensification, a heterogeneous model is developed. Intraparticle diffusion resistances, assuming both isothermal and non-isothermal conditions, are considered. It is found that intraparticle diffusion resistances are significant and should be taken into consideration, as they not only retard the chemical reactions, but also the driving forces for permeation, as well as the heat transfer. The homogenous model used earlier by the authors to optimize the membrane reactor of interest results in overestimation of both the styrene yield and the nitrobenzene conversion in the integrated reactor by 5–15% of their actual values. Hence, if possible, the full model should preferably be used in any further optimization studies.

Acknowledgements

The authors are very grateful to the Saudi Government and King Fahd University of Petroleum & Minerals (KFUPM) for sponsoring the studies of N. Abo-Ghander at the University of British Columbia. Work of F. Logist and J.F.M. Van Impe is supported in part by Projects OT/10/035, OPTEC (Center-of-Excellence Optimization in Engineering) PFV/10/02 and SCORES4CHEM KP/09/005 of the Katholieke Universiteit Leuven, FWO KAN2013 1.5.189.13, FWO-G.0930.13 of the Research Foundation Flanders (FWO) and by the Belgian Program on Interuniversity Poles of Attraction (IAP VII/19 (DYSCO)), initiated by the Belgian Federal Science Policy Office. J.F.M. Van Impe holds the Safety Engineering Chair sponsored by the Belgian Chemistry and Life Sciences Federation Essenscia.

References

[1] E.H. Stitt, Multifunctional reactors? 'Up to a point lord copper', Chem. Eng. Res. Des. 82 (2004) 129–139.
[2] C. Fukuhara, A. Igarashi, Performance simulation of a wall-type reactor in which exothermic and endothermic reactions proceed simultaneously, comparing with that of a fixed-bed reactor, Chem. Eng. Sci. 60 (2005) 6824–6834.
[3] M.E.E. Abashar, Coupling of ethylbenzene dehydrogenation and benzene hydrogenation reactions in fixed bed catalytic reactors, Chem. Eng. Process. 43 (2004) 1195–1202.
[4] B.K. Abdalla, S.S.E.H. Elnashaie, A membrane reactor for the production of styrene from ethylbenzene, J. Membr. Sci. 85 (1993) 229–239.
[5] B.K. Abdalla, S.S.E.H. Elnashaie, Catalytic dehydrogenation of ethylbenzene to styrene in membrane reactors, AIChE J. 40 (1994) 2055–2059.
[6] B.K. Abdalla, S.S.E.H. Elnashaie, Fluidized bed reactors without and with selective membranes for the catalytic dehydrogenation of ethylbenzene to styrene, J. Membr. Sci. 101 (1995) 31–42.
[7] C. Hermann, P. Quicker, R. Dittmeyer, Mathematical simulation of catalytic dehydrogenation of ethylbenzene to styrene in a composite palladium membrane reactor, J. Membr. Sci. 136 (1997) 161–172.
[8] S.S.E.H. Elnashaie, T. Moustafa, T. Alsoudani, S.S. Elshishini, Modeling and basic characteristics of novel integrated dehydrogenation-hydrogenation membrane catalytic reactors, Comput. Chem. Eng. 24 (2000) 1293–1300.
[9] T.M. Moustafa, S.S.E.H. Elnashaie, Simultaneous production of styrene and cyclohexane in an integrated membrane reactor, J. Membr. Sci. 178 (2000) 171–184.
[10] N. Abo-Ghander, J.R. Grace, S.S.E.H. Elnashaie, C.J. Lim, Modeling of a novel membrane reactor to integrate dehydrogenation of ethylbenzene to styrene with hydrogenation of nitrobenzene to aniline, Chem. Eng. Sci. 63 (2008) 1817–1826.
[11] M. Van Sint Annaland, H.A.R. Scholts, J.A.M. Kuipers, W.P.M. Van Swaaij, A novel reverse flow reactor coupling endothermic and exothermic reactions. Part II: sequential reactor configuration for reversible endothermic reactions, Chem. Eng. Sci. 57 (2002) 855–872.
[12] M. Van Sint Annaland, R.C. Nijssen, A novel reverse flow reactor coupling endothermic and exothermic reactions: an experimental study, Chem. Eng. Sci. 57 (2002) 4967–4985.
[13] B. Glöckler, G. Kolios, G. Eigenberger, Analysis of a novel reverse-flow reactor concept for autothermal methane steam reforming, Chem. Eng. Sci. 58 (2003) 593–601.

[14] D. Czechowicz, K. Skutil, A. Torz, M. Taniewski, An integrated process of oxidative coupling of methane and pyrolysis of naphtha in a scaled-up unit, J. Chem. Technol. Biotechnol. 79 (2004) 182–186.
[15] M.E.E. Abashar, Modeling and simulation of an integrated multi-shell fixed bed membrane reactor with well-mixed catalyst pattern for production of styrene and cyclohexane, Chem. Eng. Process. 50 (2011) 931–939.
[16] S.S.E.H. Elnashaie, B.K. Abdalla, R. Hughes, Simulation of the industrial fixed bed catalytic reactor for the dehydrogenation of ethylbenzene to styrene: heterogeneous dusty gas model, Ind. Eng. Chem. Res. 32 (1993) 2537–2541.
[17] B. Amon, H. Redlingshöfer, E. Klemm, E. Dieterich, G. Emig, Kinetic investigations of the deactivation by coking of a noble metal catalyst in the catalytic hydrogenation of nitrobenzene using a catalytic wall reactor, Chem. Eng. Process. 38 (1999) 395–404.
[18] S.S.E.H. Elnashaie, S.S. Elshishini, Modelling, Simulation and Optimization of Industrial Fixed Bed Catalytic Reactors, Gordon and Breach Science Publisher, Singapore, 1993.
[19] R.B. Bird, W.E. Stewart, E.N. Lightfoot, Transport Phenomena, Wiley, New York, 1960.
[20] N.S. Abo-Ghander, F. Logist, J.R. Grace, J.F.M. Van Impe, S.S.E.H. Elnashaie, C.J. Lim, Optimal design of an autothermal membrane reactor coupling the dehydrogenation of ethylbenzene to styrene with the hydrogenation of nitrobenzene to aniline, Chem. Eng. Sci. 65 (2010) 3113–3127.
[21] F. Logist, P. Van Erdeghem, J. Van Impe, Efficient deterministic multiple objective optimal control of (bio)chemical processes, Chem. Eng. Sci. 64 (11) (2009) 2527–2538.